A contrastive study on the influences of radial and three-dimensional satellite gravity gradiometry on the accuracy of the Earth's gravitational field recovery*

Zheng Wei(郑 伟)[a)†], Hsu Hou-Tse(许厚泽)[a)], Zhong Min(钟 敏)[a)], and Yun Mei-Juan(员美娟)[b)]

[a)] *State Key Laboratory of Geodesy and Earth's Dynamics, Institute of Geodesy and Geophysics, Chinese Academy of Sciences, Wuhan* 430077, *China*

[b)] *Department of Applied Physics, Wuhan University of Science and Technology, Wuhan* 430081, *China*

(Received 24 February 2012; revised manuscript received 3 May 2012)

The accuracy of the Earth's gravitational field measured from the gravity field and steady-state ocean circulation explorer (GOCE), up to 250 degrees, influenced by the radial gravity gradient V_{zz} and three-dimensional gravity gradient V_{ij} from the satellite gravity gradiometry (SGG) are contrastively demonstrated based on the analytical error model and numerical simulation, respectively. Firstly, the new analytical error model of the cumulative geoid height, influenced by the radial gravity gradient V_{zz} and three-dimensional gravity gradient V_{ij} are established, respectively. In 250 degrees, the GOCE cumulative geoid height error measured by the radial gravity gradient V_{zz} is about $2^{1/2}$ times higher than that measured by the three-dimensional gravity gradient V_{ij}. Secondly, the Earth's gravitational field from GOCE completely up to 250 degrees is recovered using the radial gravity gradient V_{zz} and three-dimensional gravity gradient V_{ij} by numerical simulation, respectively. The study results show that when the measurement error of the gravity gradient is $3\times10^{-12}/\mathrm{s}^2$, the cumulative geoid height errors using the radial gravity gradient V_{zz} and three-dimensional gravity gradient V_{ij} are 12.319 cm and 9.295 cm at 250 degrees, respectively. The accuracy of the cumulative geoid height using the three-dimensional gravity gradient V_{ij} is improved by 30%–40% on average compared with that using the radial gravity gradient V_{zz} in 250 degrees. Finally, by mutual verification of the analytical error model and numerical simulation, the orders of magnitude from the accuracies of the Earth's gravitational field recovery make no substantial differences based on the radial and three-dimensional gravity gradients, respectively. Therefore, it is feasible to develop in advance a radial cold-atom interferometric gradiometer with a measurement accuracy of $10^{-13}/\mathrm{s}^2$–$10^{-15}/\mathrm{s}^2$ for precisely producing the next-generation GOCE Follow-On Earth gravity field model with a high spatial resolution.

Keywords: GOCE, GOCE Follow-On, radial and three-dimensional gravity gradients, satellite gravity gradiometry, Earth's gravitational field

PACS: 91.10.–v **DOI:** 10.1088/1674-1056/21/10/109101

1. Introduction

The Earth's static and time-varying gravitational field can reflect the spatial distribution, movement, and change of materials on and inside the Earth, and can dominate the undulation and change of the geoid. Therefore, investigations on the fine structure and time-variable characteristics of the Earth's gravitational field are not only a requirement of geophysics, geodesy, astronomy, space science, etc., but also provide important information for resource exploration, environmental protection and disaster monitoring.

Since the Italian physicist Galileo first surveyed gravity at the end of the 16th century, many international scholars have carried out extensive gravity studies.[1−28] Instead of using the twin gravity recovery and climate experiment (GRACE) satellites to determine the Earth's medium-long-wavelength gravitational field, the European Space Agency (ESA) suc-

*Project supported by the Main Direction Program of Knowledge Innovation of the Chinese Academy of Sciences for Distinguished Young Scholars (Grant No. KZCX2-EW-QN114), the National Natural Science Foundation of China for Young Scholars (Grant Nos. 41004006, 41131067, and 11173049), the Merit-Based Scientific Research Foundation of the State Ministry of Human Resources and Social Security of China for Returned Overseas Chinese Scholars (Grant No. 2011), the Open Research Fund Program of the Key Laboratory of Computational Geodynamics of the Chinese Academy of Sciences (Grant No. 2011-04), the Frontier Field Program of Knowledge Innovation of Institute of Geodesy and Geophysics of the Chinese Academy of Sciences, and the Open Fund of State Key Laboratory of Oil and Gas Reservoir Geology and Exploitation (Grant No. PLN1113).

†Corresponding author. E-mail: wzheng@asch.whigg.ac.cn

© 2012 Chinese Physical Society and IOP Publishing Ltd

cessfully used the dedicated satellite gravity gradiometry (SGG) mission from the gravity field and steady-state ocean circulation explorer (GOCE) to precisely map the Earth's medium-short-wavelength gravitational field. The GOCE satellite was launched in 2009 and it was designed to be almost circular with an eccentricity of 0.001, near polar with an inclination of 96.5° and to have a sun-synchronous orbit. During a 20-month flight mission, the orbital altitude descends from 250 km to 240 km.[29−32] GOCE exploits the satellite-to-satellite high/low tracking (SST-HL) associated with the SGG, and except for accurately tracking the low-orbit GOCE satellite with a measuring precision of 1 cm using the high-orbit global positioning system (GPS) and the global navigation satellite system (GLONASS),[33] the second-order derivatives of the geopotential are highly accurately measured by the space-borne gradiometer with a measurement accuracy of $3\times10^{-12}/\mathrm{s}^2$ located at the satellite's centre of mass.[34,35] GOCE uses the drag-free control (DFC) technique: firstly, the linear acceleration of the satellite's centre of mass and the angular acceleration of the satellite flatform induced by non-conservative forces (e.g. atmospheric drag, solar radiation pressure, Earth's albedo, orbit altitude, and attitude control forces, etc.) are determined by the gradiometer; secondly, the non-conservative forces acting on the satellite are precisely compensated by the drag-free ion thruster (DFIT) associated with the attitude data of the satellite platform.[36] Because the influence of the non-conservative force is efficiently deducted from the SGG observations, the accuracy of the Earth's gravitational field recovery is highly improved. Since Eötvös[37] designed the first gradiometer (Eötvös torsion balance) at the beginning of the 20th century, the gradiometers have developed from monoaxial rotation to triaxial orientation, from room temperature to low temperatures (below 4.2 K) and from torsion and electrostatic suspension to superconduction and cold-atom interferometry, and the measurement accuracy of the gradiometer has also been increasingly improved.[38] Due to the sharp signal attenuation $(R_\mathrm{e}/r)^l$ of the Earth's gravitational field with the increase of orbital altitude, the Earth's medium-long-wavelength gravitational field is measured just through the perturbation analysis of the satellite orbit. However, the SGG may directly determine the second-order derivatives of the geopotential, and the spherical harmonic coefficients are enlarged l^2 times. Accordingly, the SGG can greatly suppress the signal attenuation effect of the geopotential with an increase of the orbital altitude and precisely map the Earth's medium-high-frequency gravitational field.[39] The GOCE satellite was originally planned to be launched in 2004 by the ESA. However, due to the actual measuring accuracy of the space-borne triaxial electrostatically suspended gradiometer being lower than the expected measuring accuracy of $3\times10^{-12}/\mathrm{s}^2$ and the inherent difficulty in developing the SGG system, the planned launching time of the GOCE satellite has been put off at least 6 times.

Because the GOCE mission plans to end by 2013 and greatly improving the measurement accuracy of the Earth's medium-short-wavelength gravitational field is urgently required by the interdisciplinary fields of geodesy, geophysics, etc., many international research institutes are promoting the next-generation SGG mission from GOCE Follow-On at present. A lot of scholars closely follow the hotspots and development trends of the international SGG mission, and actively throw themselves into the required demonstration and payload development of the next-generation SGG mission. Due to the lower accuracy requirements of the satellite orbit determination in the next-generation SGG mission, the ultra-precise measurement of the space-borne gradiometer is very important for accurately developing a high-degree Earth gravity field model with high spatial resolution. Because the cold-atom interferometric gradiometer is highly sensitive to the Earth's mass distribution,[40−42] the highly-accurate and high-resolution measurement of Earth's gravitational field from GOCE Follow-On will be achieved by the space-borne cold-atom interferometric gradiometer.

At present, a lot of scholars have carried out extensive and in-depth studies on the theory and methodology of recovering the Earth's gravitational field using the SGG principle.[43−49] However, comparative research of the one-dimensional and three-dimensional SGG have not yet been conducted in depth. Differently from previous studies, we contrastively demonstrate the influence of the radial and three-dimensional gravity gradients on the accuracy of the Earth's gravitational field from GOCE completely up to 250 degrees based on the new analytical error model and the numerical simulation in this paper, respectively. We propose to develop in advance a one-dimensional space-borne cold-atom interferomet-

ric gradiometer for the next-generation GOCE Follow-On mission in China for properly reducing the difficulty in developing the cold-atom interferometric gradiometer and avoiding the waste of manpower, material resources, and financial resources. This study can provide not only the theoretical and calculational basis for the optimal design of the future cold-atom interferometric gradiometer in China, but also some reference for the development direction of the next-generation lunar and planetary (e.g. Mars) gravity gradiometry missions in the solar system.

2. New analytical error models

In the Earth-fixed frame (EFF), the spherical harmonic expansion of the Earth's disturbing potential is defined as

$$T(r,\theta,\lambda) = \frac{GM}{R_e}\sum_{l=2}^{L}\left(\frac{R_e}{r}\right)^{l+1}\sum_{m=0}^{l}(\bar{C}_{lm}\cos m\lambda + \bar{S}_{lm}\sin m\lambda)\bar{\mathrm{P}}_{lm}(\cos\theta), \quad (1)$$

where GM represents the product of the Earth's mass M and the universal gravitational constant G; R_{e} shows the Earth's mean radius; $r = \sqrt{x^2+y^2+z^2}$ is the geocentric radius of the satellite, and x, y, z are three scalar components of the orbital position vector $\boldsymbol{r}$; θ and λ are the geocentric colatitude and longitude; $\bar{\mathrm{P}}_{lm}(\cos\theta)$ denotes the normalized Legendre polynomials of degree l and order m; L is the maximum spherical harmonic degree; $(\bar{C}_{lm}, \bar{S}_{lm})$ are the estimated normalized geopotential coefficients.

The second-order derivatives of $V(r,\theta,\lambda)$ with respect to x, y, z are represented as

$$\frac{\partial^2 T}{\partial x \partial y} = \begin{bmatrix} T_{xx} & T_{xy} & T_{xz} \\ T_{yx} & T_{yy} & T_{yz} \\ T_{zx} & T_{zy} & T_{zz} \end{bmatrix}, \quad (2)$$

where the second-order derivatives of the Earth's disturbing potential are the traceless symmetrical tensors, $T_{xx} + T_{yy} + T_{zz} = 0$. Therefore, only five of the nine gravity gradients are independent. The nine tensors of the SGG are expressed as

$$\begin{cases} T_{xx}(r,\theta,\lambda) = \dfrac{1}{r}T_r(r,\theta,\lambda) + \dfrac{1}{r^2}T_{\theta\theta}(r,\theta,\lambda), \\ T_{yy}(r,\theta,\lambda) = \dfrac{1}{r}T_r(r,\theta,\lambda) + \dfrac{1}{r^2}\cot\theta T_\theta(r,\theta,\lambda) + \dfrac{1}{r^2\sin^2\theta}T_{\lambda\lambda}(r,\theta,\lambda), \\ T_{zz}(r,\theta,\lambda) = T_{rr}(r,\theta,\lambda), \\ T_{xy}(r,\theta,\lambda) = T_{yx}(r,\theta,\lambda) = \dfrac{1}{r^2\sin\theta}[-\cot\theta T_\lambda(r,\theta,\lambda) + T_{\theta\lambda}(r,\theta,\lambda)], \\ T_{xz}(r,\theta,\lambda) = T_{zx}(r,\theta,\lambda) = \dfrac{1}{r^2}T_\theta(r,\theta,\lambda) - \dfrac{1}{r}T_{r\theta}(r,\theta,\lambda), \\ T_{yz}(r,\theta,\lambda) = T_{zy}(r,\theta,\lambda) = \dfrac{1}{r\sin\theta}\left[\dfrac{1}{r}T_\lambda(r,\theta,\lambda) - T_{r\lambda}(r,\theta,\lambda)\right], \end{cases} \quad (3)$$

where the first-order derivative of the Earth's disturbing potential with respect to r, θ, λ are denoted as

$$\begin{cases} T_r(r,\theta,\lambda) = -\dfrac{GM}{R_{\mathrm{e}}^2}\sum\limits_{l=2}^{L}(l+1)\left(\dfrac{R_{\mathrm{e}}}{r}\right)^{l+2}\sum\limits_{m=0}^{l}(\bar{C}_{lm}\cos m\lambda + \bar{S}_{lm}\sin m\lambda)\bar{\mathrm{P}}_{lm}(\cos\theta), \\ T_\theta(r,\theta,\lambda) = -\dfrac{GM}{R_{\mathrm{e}}}\sum\limits_{l=2}^{L}\left(\dfrac{R_{\mathrm{e}}}{r}\right)^{l+1}\sum\limits_{m=0}^{l}(\bar{C}_{lm}\cos m\lambda + \bar{S}_{lm}\sin m\lambda)\bar{\mathrm{P}}'_{lm}(\cos\theta)\sin\theta, \\ T_\lambda(r,\theta,\lambda) = \dfrac{GM}{R_{\mathrm{e}}}\sum\limits_{l=2}^{L}(\dfrac{R_{\mathrm{e}}}{r})^{l+1}\sum\limits_{m=0}^{l}m(-\bar{C}_{lm}\sin m\lambda + \bar{S}_{lm}\cos m\lambda)\bar{\mathrm{P}}_{lm}(\cos\theta), \end{cases} \quad (4)$$

the second-order derivatives of the Earth's disturbing potential with respect to r, θ, λ are given as

$$\begin{cases} T_{rr}(r,\theta,\lambda) = \dfrac{GM}{R_{\rm e}^3}\sum\limits_{l=2}^{L}(l+1)(l+2)\left(\dfrac{R_{\rm e}}{r}\right)^{l+3}\sum\limits_{m=0}^{l}(\bar{C}_{lm}\cos m\lambda + \bar{S}_{lm}\sin m\lambda)\bar{\rm P}_{lm}(\cos\theta), \\ T_{\theta\theta}(r,\theta,\lambda) = \dfrac{GM}{R_{\rm e}}\sum\limits_{l=2}^{L}\left(\dfrac{R_{\rm e}}{r}\right)^{l+1}\sum\limits_{m=0}^{l}(\bar{C}_{lm}\cos m\lambda + \bar{S}_{lm}\sin m\lambda)[\bar{\rm P}''_{lm}(\cos\theta)\sin^2\theta - \bar{\rm P}'_{lm}(\cos\theta)\cos\theta], \\ T_{\lambda\lambda}(r,\theta,\lambda) = -\dfrac{GM}{R_{\rm e}}\sum\limits_{l=2}^{L}\left(\dfrac{R_{\rm e}}{r}\right)^{l+1}\sum\limits_{m=0}^{l}m^2(\bar{C}_{lm}\cos m\lambda + \bar{S}_{lm}\sin m\lambda)\bar{\rm P}_{lm}(\cos\theta), \\ T_{r\theta}(r,\theta,\lambda) = T_{\theta r}(r,\theta,\lambda) = \dfrac{GM}{R_{\rm e}^2}\sum\limits_{l=2}^{L}(l+1)\left(\dfrac{R_{\rm e}}{r}\right)^{l+2}\sum\limits_{m=0}^{l}(\bar{C}_{lm}\cos m\lambda + \bar{S}_{lm}\sin m\lambda)\bar{\rm P}'_{lm}(\cos\theta)\sin\theta, \\ T_{r\lambda}(r,\theta,\lambda) = T_{\lambda r}(r,\theta,\lambda) = \dfrac{GM}{R_{\rm e}^2}\sum\limits_{l=2}^{L}(l+1)\left(\dfrac{R_{\rm e}}{r}\right)^{l+2}\sum\limits_{m=0}^{l}m(\bar{C}_{lm}\sin m\lambda - \bar{S}_{lm}\cos m\lambda)\bar{\rm P}_{lm}(\cos\theta), \\ T_{\theta\lambda}(r,\theta,\lambda) = T_{\lambda\theta}(r,\theta,\lambda) = \dfrac{GM}{R_{\rm e}}\sum\limits_{l=2}^{L}\left(\dfrac{R_{\rm e}}{r}\right)^{l+1}\sum\limits_{m=0}^{l}m(\bar{C}_{lm}\sin m\lambda - \bar{S}_{lm}\cos m\lambda)\bar{\rm P}'_{lm}(\cos\theta)\sin\theta, \end{cases} \tag{5}$$

the zero-order, first-order, and second-order derivatives of the Legendre function are expressed as

$$\begin{cases} \bar{\rm P}_{lm}(\cos\theta) = \gamma_m 2^{-l}\sin^m\theta\sum\limits_{k=0}^{[(l-m)/2]}(-1)^k\dfrac{(2l-2k)!}{k!(l-k)!(l-m-2k)!}(\cos\theta)^{l-m-2k}, \quad (m\le l), \\ \bar{\rm P}'_{lm}(\cos\theta) = \dfrac{1}{\sin\theta}[(l+1)\cos\theta\bar{\rm P}_{lm}(\cos\theta) - (l-m-1)\bar{\rm P}_{l+1,m}(\cos\theta)], \\ \bar{\rm P}''_{lm}(\cos\theta) = -l\bar{\rm P}_{lm}(\cos\theta) + l\cos\theta\bar{\rm P}'_{l-1,m}(\cos\theta) + \dfrac{l}{4}\cos^2\theta[\bar{\rm P}'_{l-1,m+1}(\cos\theta) - 4\bar{\rm P}'_{l-1,m-1}(\cos\theta)], \end{cases} \tag{6}$$

where

$$\gamma_m = \begin{cases} \sqrt{2(2l+1)\dfrac{(l-|m|)!}{(l+|m|)!}}, & (m\ne 0), \\ \sqrt{2l+1}, & (m=0). \end{cases}$$

The analytical formula of the radial gravity gradient by a combination of Eqs. (3) and (5) are shown as

$$(\bar{C}_{lm},\bar{S}_{lm}) = \frac{R_{\rm e}^3}{4\pi GM}\left(\frac{r}{R_{\rm e}}\right)^{l+3}(l+1)^{-1}(l+2)^{-1} \times \iint\limits_{\sigma} T_{zz}\bar{\rm Y}_{lm}(\theta,\lambda)\,{\rm d}\sigma, \tag{7}$$

where T_{zz} is the radial gravity gradient calculated by the discrete numerical integration. The Earth's surface is equably plotted out by $\Delta\theta$ and $\Delta\lambda$, and the mean radial gravity gradients $\bar{T}_{zz}\big|_{ij}$ within each grid are obtained, where i and j are the longitude and latitude labels of the grid. Therefore, equation (7) can be modified into

$$(\bar{C}_{lm},\bar{S}_{lm}) = \frac{R_{\rm e}^3}{4\pi GM}\left(\frac{r}{R_{\rm e}}\right)^{l+3}(l+1)^{-1}(l+2)^{-1} \times \sum_{i,j}\bar{T}_{zz}\big|_{ij}\iint\limits_{\sigma_{ij}}\bar{\rm Y}_{lm}(\theta,\lambda)\,{\rm d}\sigma_{ij}, \tag{8}$$

where ${\rm d}\sigma_{ij} = \sin\theta{\rm d}\theta{\rm d}\lambda$.

The cumulative geoid height errors are defined as

$$\sigma_N^L = R_{\rm e}\sqrt{\sum_{l=2}^{L}\sum_{m=0}^{l}(\delta\bar{C}_{lm})^2 + (\delta\bar{S}_{lm})^2}, \tag{9}$$

where $\delta\bar{C}_{lm}$ and $\delta\bar{S}_{lm}$ are the accuracies of the geopotential coefficients.

Because a large amount of data can effectively reduce the observation noise, if the number of the radial gravity gradient T_{zz} of the global uniform distribution is N_0 and the errors of T_{zz} meet the random features of normal distribution, the variance of the geopotential coefficients is proportional to $1/N_0$. By combining Eqs. (8) and (9), based on the orthonormality of the spherical harmonic function

$$\left[\frac{1}{4\pi}\iint\limits_{\sigma_{ij}}\bar{\rm Y}_{lm}(\theta,\lambda)\sin\theta{\rm d}\theta{\rm d}\lambda\right]^2 = 1$$

and $\sum\limits_{m=0}^{l} = 2l+1$, the analytical error model of the cumulative geoid height influenced by the radial gravity gradient T_{zz} is expressed as

$$\begin{aligned}&\sigma_N(T_{zz}) \\ \approx\ & R_{\rm e}\frac{\sigma_\gamma}{GM/R_{\rm e}^3} \\ &\times\sqrt{\sum_{l=2}^{L}\frac{2l+1}{(l+1)^2(l+2)^2}\left(\frac{r}{R_{\rm e}}\right)^{2(l+3)}\frac{1}{N_0}},\end{aligned} \tag{10}$$

where σ_γ is the measurement accuracy of the gravity gradient.

The analytical formulas of the horizontal gravity gradients $T_{xx(yy)}$ by a combination of Eqs. (3), (4), and (5) are denoted as

$$\begin{aligned}&(\bar{C}_{lm}, \bar{S}_{lm})\\ &= \frac{R_{\rm e}^3}{4\pi GM}\left(\frac{r}{R_{\rm e}}\right)^{l+3}(l+1)^{-1}(m-l-1)^{-1}\\ &\quad\times \iint\limits_{\sigma} T_{xx(yy)}\bar{\rm Y}_{lm}(\theta,\lambda)\,{\rm d}\sigma. \end{aligned} \tag{11}$$

By a combination of Eqs. (9) and (11), based on the orthonormality of the spherical harmonic function, the analytical error models of the cumulative geoid height, influenced by the horizontal gravity gradient T_{xx} and T_{yy} are indicated as

$$\begin{aligned}&\sigma_N(T_{xx})\\ &\approx \sigma_N(T_{yy}) \approx R_{\rm e}\frac{\sigma_\gamma}{GM/R_{\rm e}^3}\\ &\quad\times\sqrt{\sum_{l=2}^{L}\frac{2l+1}{\dfrac{4(l+1)^3(l+2)(2l+3)}{9(2l+1)}}\left(\frac{r}{R_{\rm e}}\right)^{2(l+3)}\frac{1}{N_0}}. \end{aligned} \tag{12}$$

As illustrated in Fig. 1, the dashed and solid lines represent, respectively, the GOCE cumulative geoid height errors up to 250 degrees from the radial gravity gradient T_{zz} (see Eq. (10)) and horizontal gravity gradient T_{ij} (see Eq. (12)) based on the analytical error model method with a measurement error of a space-borne gradiometer, $3\times10^{-12}/{\rm s}^2$, an orbital altitude of 250 km, an observation duration of 60 days and a sampling interval of 5 s. The result shows that the influence of the radial gravity gradient T_{zz} on the accuracy of the Earth's gravitational field recovery is greater than that of the horizontal gravity gradient $T_{xx(yy)}$. Therefore, the radial gravity gradient T_{zz} is the most dominating component in the nine gravity gradient tensors.

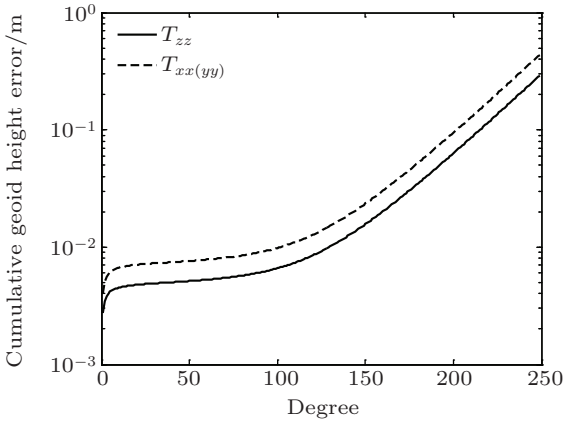


Fig. 1. GOCE cumulative geoid height errors from radial gravity gradient T_{zz} and horizontal gravity gradient $T_{xx(yy)}$ based on the analytical method.

As shown in Eq. (2), three diagonal tensors T_{xx}, T_{yy}, and T_{zz} are the main components in the nine gravity gradients, and the influence of the non-diagonal tensors on the accuracy of the Earth's gravitational field can be ignored with respect to those of the diagonal tensors. Therefore, by a combination of Eqs. (3), (4), (5), and (9), based on the orthonormality of the spherical harmonic function, the analytical error model of the cumulative geoid height influenced by the three-dimensional gravity gradients $T_{ij} = (T_{xx}, T_{yy}, T_{zz})$ are given as

$$\sigma_N(T_{ij}) \approx R_{\rm e}\frac{\sigma_\gamma}{GM/R_{\rm e}^3}\sqrt{\sum_{l=2}^{L}\frac{2l+1}{\left[(l+1)^2(l+2)^2+\dfrac{8(l+1)^3(l+2)(2l+3)}{9(2l+1)}\right]}\left(\frac{r}{R_{\rm e}}\right)^{2(l+3)}\frac{1}{N_0}}. \tag{13}$$

The mean ratio of the influence of the radial gravity gradient T_{zz} to the influence of the three-dimensional gravity gradient T_{ij} on the cumulative geoid height error is expressed as

$$\text{Mean}\,[\sigma_N(T_{zz})/\sigma_N(T_{ij})] \approx \sqrt{2}. \tag{14}$$

3. Numerical simulation

In the Earth-centred inertial (ECI) frame, the observation equation of the satellite is established as

$$\boldsymbol{y}_{k\times1} = \boldsymbol{A}_{k\times n}\cdot\bar{\boldsymbol{x}}_{n\times1}, \tag{15}$$

where $\boldsymbol{y}_{k\times1}$ denotes the SGG observations, k represents the number of the SGG observation points; $\boldsymbol{A}_{k\times n}$ shows a design matrix with m rows and n columns, $n = L^2 + 2L - 3$; $\bar{\boldsymbol{x}}_{n\times1}$ expresses the estimated geopotential coefficients.

The specific processes for mapping the Earth's gravitational field from GOCE completely up to 250 degrees using the time-space-wise approach are shown in Ref. [50]. As illustrated in Fig. 2, firstly, the four equidistant and regular reference spherical surfaces $\boldsymbol{r}_1$, $\boldsymbol{r}_2$, $\boldsymbol{r}_3$, and $\boldsymbol{r}_4$ with the centre of the sphere located at the geocenter are designed and the orbit of the GOCE satellite is located between the second and third reference spherical surfaces. The gridding is equably plotted out by the longitude and latitude on each reference spherical surface. Secondly, the SGG data are rapidly derived from the Fast Fourier Transform (FFT) on each reference spherical surface and are transformed from the reference spherical surfaces to the satellite orbit (the space-wise approach). Finally, equation (15) is solved at the satellite orbit, and the geopotential coefficients are fitted by the least-squares procedure (the time-wise approach).

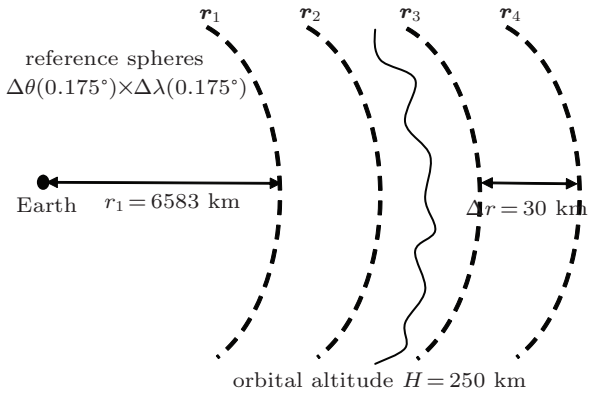


Fig. 2. Schematic diagram of the Earth's gravitational field determined from GOCE using the time-space-wise method.

Table 1. Numerical simulation parameters of the GOCE orbit.

Parameters	Indexes
Reference model	EGM2008
Orbital altitude	250 km
Orbital inclination	96.5°
Orbital eccentricity	0.001
Observation duration	60 days
Sampling interval	5 s

We firstly simulate the ephemerides of the GOCE satellite using numerical integration formulas of the 9th-order Runge–Kutta linear single-step method associated with the 12th-order Adams–Cowell linear multi-step method. The parameters of the numerical simulation from the GOCE orbit are listed in Table 1.

As indicated in Fig. 3, the intersected line represents the accuracy of the Earth gravity field model GO_CONS_GCF_2_DIR_R1 completely up to 240 degrees released by the French Centre National d'Études Spatiales (CNES) using the 2-month real GOCE observations based on the direct method. At 240 degrees, the cumulative geoid height error is 8.523 cm. The solid and dashed lines denote the accuracies of the Earth's gravitational field from GOCE completely up to 250 degrees based on the radial gravity gradient T_{zz} and the three-dimensional gravity gradient T_{ij} of the SGG observations, respectively, where the measurement error of the SGG observations is $3\times10^{-12}/\mathrm{s}^2$. The statistical results of the cumulative geoid height errors using the radial gravity gradient T_{zz} and the three-dimensional gravity gradient T_{ij} are listed in Table 2. The simulated results show firstly, the cumulative geoid height error is 9.295 cm at 250 degrees using the three-dimensional gravity gradient T_{ij}, which preferably fits with the Earth gravity field model GO_CONS_GCF_2_DIR_R1.[51] The cumulative geoid height error is 12.319 cm at 250 degrees using the radial gravity gradient T_{zz}. Secondly, the accuracy of the cumulative geoid height by the three-dimensional gravity gradient T_{ij} is improved by 30%–40% on average, compared with that measured with the radial gravity gradient T_{zz} at 250 degrees.

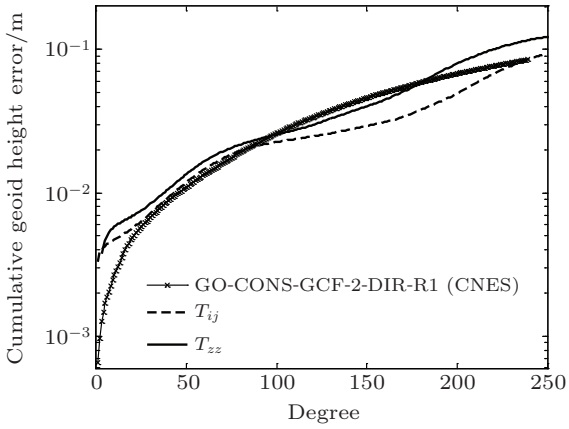


Fig. 3. A comparison of cumulative geoid height errors from GOCE between the radial gravity gradient T_{zz} and the three-dimensional gravity gradient T_{ij} based on the numerical simulation method.

Table 2. Statistics of the cumulative geoid height errors based on different gravity gradients of SGG.

Gravity gradients	Cumulative geoid height errors (10^{-2} m)					
	Degree 20	Degree 50	Degree 100	Degree 150	Degree 200	Degree 250
GO_CONS_GCF_2_DIR_R1	0.471	1.076	2.570	4.571	6.751	8.523
Three-dimensional gradients T_{ij}	0.553	1.163	2.253	2.916	4.864	9.295
Radial gradient T_{zz}	0.701	1.389	2.575	4.059	8.089	12.319

4. Discussion and conclusions

Due to the difficulty in developing the three-dimensional space-borne cold-atom interferometric gradiometer with an accuracy of $10^{-13}/s^2$–$10^{-15}/s^2$ in the next-generation GOCE Follow-On mission, we take the GOCE satellite gravity gradiometry mission of the ESA as an example and carry out a comparative study on the influence of the radial gravity gradient V_{zz} and three-dimensional gravity gradient V_{ij} on the accuracy of the Earth's gravitational field completely up to 250 degrees using the analytical error model and numerical simulations, respectively.

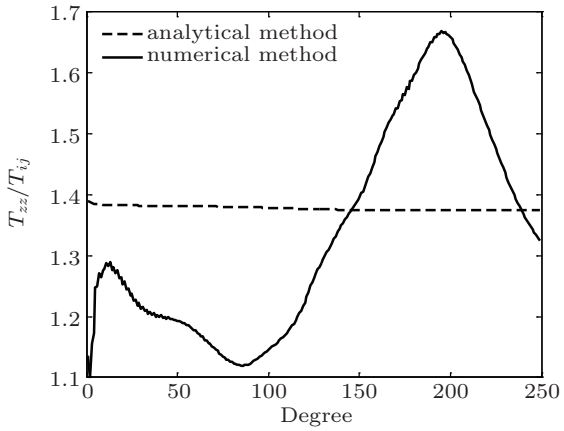


Fig. 4. Ratios between the cumulative geoid height error influenced by the radial gravity gradient T_{zz} and that influenced by the three-dimensional gravity gradient T_{ij} based on the analytical and numerical methods.

As shown in Fig. 4, the dashed and solid lines illustrate the ratios of the cumulative geoid height errors influenced by the radial gravity gradient T_{zz} and three-dimensional gravity gradient T_{ij} based on the analytical and numerical methods, respectively. The obtained results are follows:

(i) In 250 degrees, the accuracy of the cumulative geoid height from GOCE using the three-dimensional gravity gradient V_{ij} is about $2^{1/2}$ times higher than that using the radial gravity gradient V_{zz} based on the analytical error models.

(ii) In 250 degrees, the accuracy of the GOCE Earth's gravitational field from the three-dimensional gravity gradient V_{ij} is improved by 30%∼40% on average compared with that from the radial gravity gradient V_{zz} from numerical simulations.

(iii) Due to fewer differences between the accuracy of the Earth's gravitational field recovery by the radial gravity gradient and by the three-dimensional gravity gradient, we suggest developing a radial space-borne cold-atom interferometric gradiometer in China for accurately establishing the next-generation GOCE Follow-On Earth gravity field model with a high spatial resolution.

Acknowledgement

The authors greatly appreciate Professor Luo J of School of Physics, Huazhong University of Science and Technology, China for helpful and constructive discussion, and also the European Space Agency (ESA) for providing the relevant information about the GOCE satellite.

References

[1] Zhu Z H, Ge P W, Xu Z Y and Huo C R 1998 *Chin. Phys.* **7** 801

[2] Liu Y C, Chen W C, Huo C R and Ge P W 1999 *Chin. Phys.* **8** 881

[3] Zhu Z H, Ge P W and Xu Z Y 2000 *Chin. Phys.* **9** 321

[4] Chen G 2001 *Chin. Phys.* **10** 787

[5] Xu H Z 2001 *Sci. Surv. Mapp.* **26** 1 (in Chinese)

[6] Wu Y B, Li J L and Li L 2002 *Chin. Phys.* **11** 222

[7] Zhu Z H, Hong Y, Ge P W and Yu Y D 2004 *Chin. Phys.* **13** 1982

[8] Xu H Z, Zhou X H and Peng B B 2005 *Geospatial Inform.* **3** 1 (in Chinese)

[9] Zhang H W, Xu H Z and Liu X Q 2004 *Prog. Geophys.* **19** 372 (in Chinese)

[10] Shen Y Z, Xu H Z and Wu B 2005 *Chin. J. Geophys.* **48** 807 (in Chinese)

[11] Zheng W, Lu X L, Xu H Z and Luo J 2005 *Prog. Nat. Sci.* **15** 596

[12] Cheng L Y and Xu H Z 2006 *Chin. J. Geophys.* **49** 93 (in Chinese)

[13] Zhou X H, Xu H Z and Wu B 2006 *Chin. J. Geophys.* **49** 718 (in Chinese)

[14] Zheng W, Shao C G, Luo J and Xu H Z 2006 *Chin. J. Geophys.* **49** 712 (in Chinese)

[15] Zeng X X, Yang S Z and Chen D Y 2008 *Chin. Phys.* B **17** 1629

[16] Zheng W, Shao C G, Luo J and Xu H Z 2008 *Prog. Nat. Sci.* **18** 555

[17] Zheng W, Xu H Z, Zhong M and Yun M J 2008 *Chin. J. Geophys.* **51** 1704 (in Chinese)

[18] Zheng W, Xu H Z, Zhong M and Yun M J 2008 *Chin. Phys. Lett.* **25** 4482

[19] Zheng W, Xu H Z, Zhong M and Yun M J 2009 *Chin. Phys. Lett.* **26** 029101

[20] Zheng W, Xu H Z, Zhong M and Yun M J 2009 *Chin. Phys.* B **18** 3597

[21] Zheng W, Xu H Z, Zhong M and Yun M J 2009 *Chin. J. Geophys.* **52** 1465 (in Chinese)

[22] Zheng W, Xu H Z, Zhong M and Yun M J 2009 *Chin. J. Geophys.* **52** 1966 (in Chinese)

[23] Zheng W, Xu H Z, Zhong M and Yun M J 2009 *Chin. J. Geophys.* **52** 2712 (in Chinese)

[24] Zheng W, Xu H Z, Zhong M and Yun M J 2010 *Chin. J. Geophys.* **53** 796 (in Chinese)

[25] Zheng W, Xu H Z, Zhong M and Yun M J 2011 *T. Jpn. Soc. Aeronaut. S.* **54** 106

[26] Zheng W, Xu H Z, Zhong M and Yun M J 2012 *J. Geodyn.* **53** 1

[27] Zheng W, Xu H Z, Zhong M and Yun M J 2012 *IEEE Geosci. Remote. S.* **9** 422

[28] Zheng W, Xu H Z, Zhong M and Yun M J 2012 *Chin. J. Geophys.* **55** 822 (in Chinese)

[29] Aguirre-Martinez M and Sneeuw N 2003 *Space Sci. Rev.* **108** 409

[30] Muzi D and Allasio A 2003 *Acta Astronaut.* **54** 167

[31] Zheng W, Xu H Z, Zhong M and Yun M J 2010 *Sci. Surv. Mapp.* **35** 5 (in Chinese)

[32] Zheng W, Xu H Z, Zhong M and Yun M J 2010 *Sci. Surv. Mapp.* **35** 57 (in Chinese)

[33] Visser P and van den IJssel J 2000 *J. Geod.* **74** 590

[34] Albertella A, Migliaccio F and Sanso F 2002 *Celest. Mech. Dyn. Astr.* **83** 1

[35] Bian S F and Ji B 2006 *Prog. Geophys.* **21** 660 (in Chinese)

[36] Canuto E, Martella P and Sechi G 2003 *Space Sci. Rev.* **108** 357

[37] Shaw H and Lancaster-Jones 1922 *Proc. Phys. Soc. London* **35** 151

[38] Drinkwater M R, Floberghagen R and Haagmans R 2003 *Space Sci. Rev.* **108** 419

[39] Zheng W 2007 *"Theory and Methodology of Earth's Gravitational Field Recovery Based on Satellite Gravity Measurement"* [Ph. D. Thesis], Wuhan, Huazhong University of Science and Technology

[40] Jekeli C 2004 *The State of the Planet: Frontiers and Challengs in Geophysics,* Geophysical Monograph Series (Washington D.C.: AGU)

[41] Yu N, Kohel J M, Kellogg J R and Maleki L 2006 *Appl. Phys.* B **84** 647

[42] Kohel J M, Thompson R J, Kellogg J R, Aveline D C and Yu N 2008 *NASA Earth Science Technology Conference*, June 24–28, 2008, Maryland, USA

[43] Petrovskaya M S and Zielinski J B 1997 *Adv. Space Res.* **19** 1723

[44] Klees R, Koop R and Visser P 2000 *J. Geod.* **74** 561

[45] Ditmar P, Klees R and Kostenko F 2003 *J. Geod.* **76** 690

[46] Pail R and Wermuth M 2003 *Adv. Geosci.* **1** 5

[47] Wu X P and Lu Z L 1992 *Acta Geodaetica et Cartographica Sinica* **21** 123 (in Chinese)

[48] Zhang C D, Wu X P and Lu Z L 2000 *Acta Geodaetica et Cartographica Sinica* **29** 297 (in Chinese)

[49] Ning J S, Luo Z C and Chen Y Q 2002 *Eng. Sci.* **4** 23 (in Chinese)

[50] Zheng W, Xu H Z, Zhong M and Yun M J 2011 *Chin. J. Geophys.* **54** 240 (in Chinese)

[51] Bruinsma S L, Marty J C, Balmino G, Biancale R, Foerste C, Abrikosov O and Meumayer H 2010 *Proceedings of the ESA Living Planet Symposium*, June 27–July 2, 2010 Bergen, Norway, ESA, SP-686, ISBN 978-92-9221-250-6, ISSN 1609-042X, p. 1